

# Rigid Unit Modes in $sp$ - $sp^2$ Hybridized Carbon Systems: Origin of Negative Thermal Expansion

Cheol-Woon Kim, Seoung-Hun Kang, and Young-Kyun Kwon\*

*Department of Physics and Research Institute for Basic Sciences,*

*Kyung Hee University, Seoul, 02447, Korea*

(Dated: June 10, 2021)

## Abstract

Using density functional theory combined with quasi-harmonic approximation, we investigate the thermal expansion behaviors of three different types ( $\alpha$ ,  $\beta$ , and  $\gamma$ ) of graphyne which is a two-dimensional carbon allotrope composed of  $sp$  and  $sp^2$  bonds. For each type of graphyne, we obtain the temperature dependent area variation by minimizing its free energy as a function of temperature, which is calculated by considering all the phonon modes in the whole Brillouin zone. We find that all three types of graphyne exhibit negative in-plane thermal expansion up to  $T \lesssim 1000$  K. The observed in-plane thermal contraction can be attributed partially to the ripple effect, similarly in graphene. The ripple effect itself, however, is not sufficient to explain anomalously larger thermal contraction found in graphyne than in graphene. Our deliberate analysis on the phonon modes observed in graphyne enables us to discover another source causing such thermal expansion anomaly. We find that there are particular phonon modes with frequencies around a few hundreds of  $\text{cm}^{-1}$  existing exclusively in graphyne that may fill empty spaces resulting in area reduction. These modes are identified as “rigid unit modes” corresponding to the libration of each rigid unit composed of  $sp^2$  bonds.

---

\* Corresponding author. E-mail: ykkwon@khu.ac.kr

## I. INTRODUCTION

Various carbon allotropes based on  $sp^2$  hybridization, such as fullerenes, [1] nanotubes, [2] and graphene, [3] have been intensively studied during last a few decades, since their first discoveries. Their unique properties are basically related to the hexagonal geometry and the Dirac cones in the electronic structure of graphene, [4–6] which is a base material to form other  $sp^2$ -bonded carbon allotropes. To make use of graphene in future nanoelectronics, however, it is indispensable to open an energy gap at the Fermi level  $E_F$ . Although lots of attempts have been made to open a band gap, [7–12] nothing has yet come along for practical applications. As a separate approach, sundry efforts have been made to search for other 2D allotropes intrinsically possessing an energy gap at  $E_F$  to be used as graphene substitutes in electronic applications. [13]

A new 2D layered carbon allotrope called graphyne was proposed in 1987. [14] It can be geometrically generated from graphene by inserting a single acetylenic linkage (AL) consisting of two  $sp$ -hybridized carbon atoms into a bond in graphene composed of  $sp^2$ -hybridized carbon atoms only. Since there are a number of ways of inserting ALs, many different types of graphyne can be formed. Among them were mainly considered three types with a hexagonal symmetry, classified by the number of ALs attached to each  $sp^2$ -hybridized or triply-coordinated carbon atom:  $\alpha$ -,  $\beta$ -, and  $\gamma$ -graphyne. Fig. 1(a–c) shows their equilibrium structures. In  $\alpha$ -graphyne shown in Fig. 1(a), there are three ALs connected to each  $sp^2$ -hybridized carbon atom, whereas in  $\beta$ -graphyne ( $\gamma$ -graphyne), every  $sp^2$ -bonded atom has only two ALs (one AL) as shown in Fig. 1(b) and (c), respectively.

Theoretical studies reported that both  $\alpha$ - and  $\beta$ -graphyne structures possess Dirac cones near  $E_F$  in its Brillouin zone (BZ) representing their semi-metallic characteristics like in graphene. [15–21] It was also reported that  $\gamma$ -graphyne, which is by far the most stable graphyne, is interestingly an intrinsic semiconductor with a direct band gap of 0.46 eV at  $M$  points. The existence of the band gap was ascribed by the Peierls instability resulting in the wave function localization at the triple bonds. [18] It is, therefore, expected that  $\gamma$ -graphyne could be made use of as a semiconducting component in future nanoelectronics.

Although various research groups have endeavored to synthesize them, graphyne has not yet been realized in a crystalline form. Nevertheless, it was already reported that graphyne sub units that resemble  $\gamma$ -graphyne were successfully synthesized. [22–24] Moreover, one of

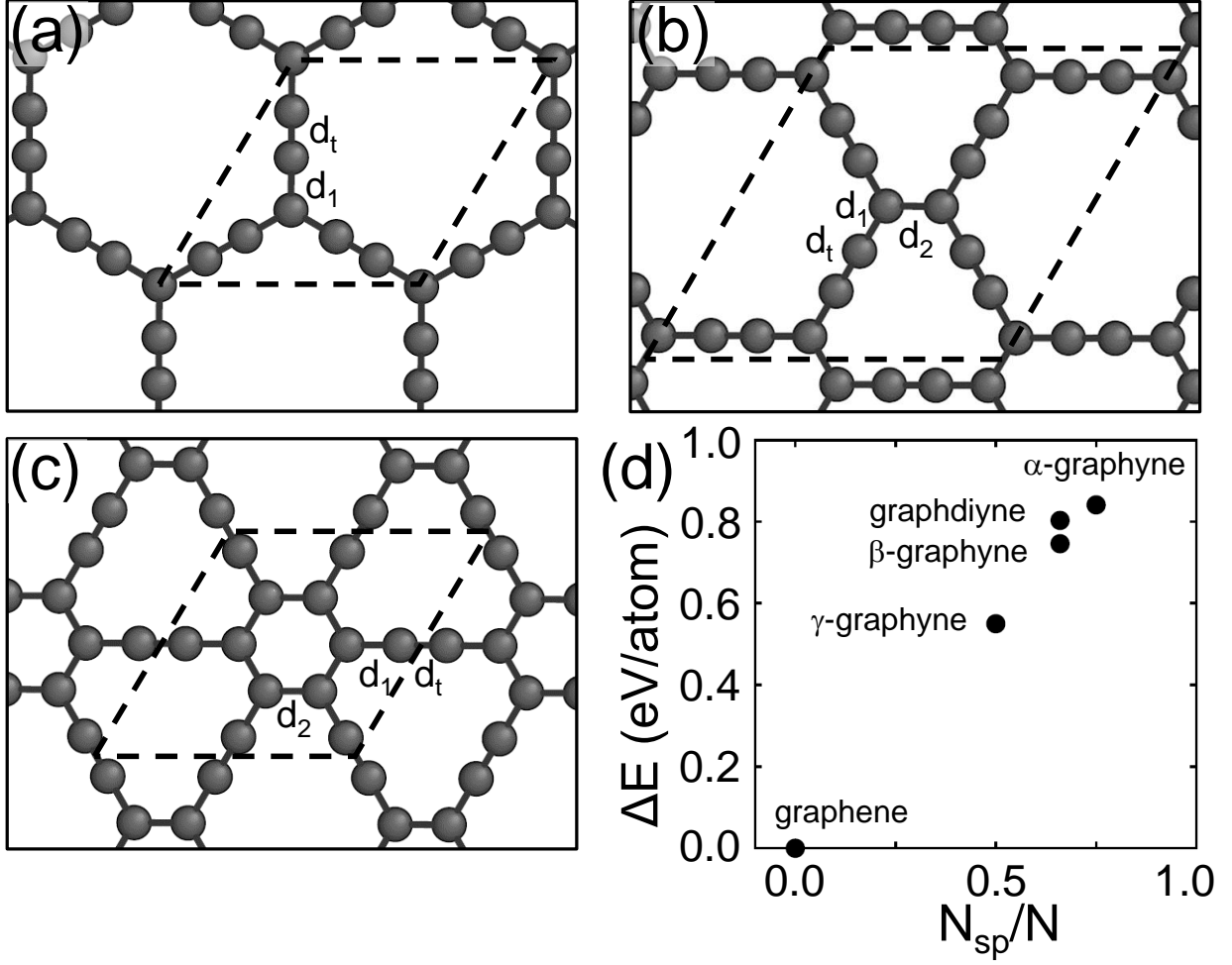


FIG. 1. Equilibrium structures of (a)  $\alpha$ -graphyne, (b)  $\beta$ -graphyne and (c)  $\gamma$ -graphyne. Respective hexagonal unit cells are depicted by dashed parallelograms. Nonequivalent bonds in each type of graphyne are denoted by  $d_1$ ,  $d_2$ , and  $d_t$ .  $d_1$  and  $d_2$ , which are single-bond like, represent a bond between an  $sp^2$ -bonded (or triply-coordinated) and an  $sp$ -bonded (or doubly-coordinated) atoms, and one between two triply-coordinated atoms, respectively, whereas  $d_t$  designates a triple bond between two  $sp$  atoms in every acetylenic linkage. (d) Cohesive energy comparison of three types of graphyne and graphdiyne with respect to graphene as a function of  $N_{sp}/N$ , where  $N_{sp}$  and  $N$  are the number of  $sp$ -bonded or doubly-coordinated atoms and  $N$  and the total number of atoms in the unit cell, respectively.

their cousin structures with two ALs in a sequence instead of a single AL in  $\gamma$ -graphyne, called graphdiyne, was also reported to be discovered in the form of sheet, [25] as well as in a tube form. [26] According to our calculation as well as other studies, [27–29]  $\beta$ -graphyne and  $\gamma$ -graphyne are even more stable than graphdiyne, as shown in Fig. 1(d), and thus expected to be synthesized in near future.

Compared to the structural and electronic properties of  $\alpha$ -,  $\beta$ -, and  $\gamma$ -graphyne that have been intensively studied as discussed above, there have been not many studies on their thermal and thermal expansion (TE) behaviors, [20, 21, 30] which are also necessary properties to be disclosed in advance for them to be utilized as various devices in future nanoelectronics.

It is well known that most materials expand thermally with a very different material-dependent linear TE coefficient (TEC) of  $10^{-7} \sim 10^{-4}$  mainly due to the atomic vibration under asymmetric potential. In almost all devices and equipment, such a TE usually becomes a critical problem deteriorating their performance and lifetime. There have been, on the other hand, several reports revealing materials with a negative TEC (NTEC), such as graphite, [31] carbon nanotubes, [32, 33] zirconium tungstate ( $\text{ZrW}_2\text{O}_8$ ), [34] perovskite oxides, [35–37] and Invar alloys, [38, 39] originating due to a ripple effect, bending/twisting modes, rigid unit modes (RUMs), [40, 41] atomic radius contraction, [42] or a magnetovolume effects. [43] Researchers have made various attempts to make composites containing NTE materials, such as  $\text{ZrW}_2\text{O}_8$  [44–46] and  $\beta$ -eucryptite [47], as a TE compensator, expecting them to be high-performance composites with near zero TE. It was indeed shown that TE can be suppressed in molten aluminum alloy with NTE manganese antiperovskites. [48]

In this letter, we report a first discovery of RUMs in two-dimensional graphitic carbon systems, which are responsible for a TE anomaly of NTE in  $sp$ - $sp^2$  hybridized carbon systems, similarly observed in 2D perovskites. [49] The thermal properties and TE behaviors of  $\alpha$ -,  $\beta$ -, and  $\gamma$ -graphyne were investigated by first-principles calculations of temperature- and volume-dependent free energies from the phonon properties. Similar to graphene, all of three configurations contract with temperature up to  $T \approx 1000$  K, but the absolute values of their TECs are much larger than that of graphene especially at low temperatures. Based on our thorough investigation on their phonon modes, we attributed such thermal contraction behaviors to not only the ripple effect as in graphene, but also RUMs corresponding to libration motions of rigid units composed of  $sp^2$ -bonds only.

## II. COMPUTATIONAL DETAILS

To investigate the TE behaviors of three types of graphyne, we first obtained their equilibrium structures by carrying out first-principles calculations within the density functional theory (DFT), [50] as implemented in Vienna *ab initio* simulation package (VASP), [51, 52] while adjusting three different carbon-carbon bonds, and thus the lattice constant of each graphyne as discussed in Sect. III. Projector augmented wave potentials [53, 54] was employed to describe the valence electrons, and the electronic wave functions were expanded by a plane wave basis set with the cutoff energy of 450 eV. The exchange-correlation functional was treated with the Perdew-Burke-Ernzerhof (PBE) parameterization [55] of the generalized gradient approximation (GGA). To mimic single-layered graphyne, we introduced a vacuum region with 15 Å along the *c*-axis perpendicular to the sheet. The BZ was sampled using a  $\Gamma$ -centered  $10 \times 10 \times 1$  *k*-grid for the primitive unit cell of each type of graphyne. Although the primitive cell size of  $\beta$ -graphyne is larger than the other types, the same *k*-grid was employed for precise calculation for  $\beta$ -graphyne because there were earlier studies on  $\beta$ -graphyne showing inconsistent results on structural stability. [20, 21]

The phonon dispersion relations were computed by applying the finite displacement method (FD) [56, 57] for  $3 \times 3 \times 1$  supercells. The corresponding reduced BZs were sampled by  $3 \times 3 \times 1$  *k*-point meshes. In each supercell, we solved the secular equation of dynamical matrix constructed at every wave vector  $\mathbf{q}$  from the force constant matrices computed under FD to obtain the phonon dispersion relation. To investigate thermal properties, we employed quasi-harmonic approximation (QHA), [58, 59] in which the Helmholtz free energy of a 2D graphyne sheet was calculated by

$$F(T, A) = U(A) + \frac{1}{2} \sum_{\mathbf{q}, n} \hbar \omega_{\mathbf{q}, n} + k_B T \sum_{\mathbf{q}, n} \ln \left\{ 1 - \exp \left( -\frac{\hbar \omega_{\mathbf{q}, n}}{k_B T} \right) \right\}, \quad (1)$$

where  $\hbar$ , and  $k_B$  are the reduced Planck constant, and the Boltzmann constant, respectively; and  $\omega_{\mathbf{q}, n}$  is the phonon frequency with the wave vectors  $\mathbf{q}$  and the mode indices *n*. In Eq. (1), the first term  $U(A)$  is the system internal energy with a constant area *A* at  $T = 0$ ; the second term represents the vibrational zero-point energy of the lattice; and the last term corresponds to the phonon contribution to the free energy in QHA. [58, 59]  $U(A)$  and  $\omega_{\mathbf{q}, n}$  were evaluated at 12 different area points.  $F(T, A)$  was fitted to the integral form of the Vinet equation of state [60] to obtain the minimum values of the thermodynamic functions with respect to

the area, and thus the equilibrium area,  $A(T)$ , as a function of temperature. TE behaviors of three types of graphyne sheets were explored by calculating the area TEC  $\alpha_S(T)$  as a function of  $T$ ,

$$\alpha_S(T) = \frac{1}{A(T)} \frac{dA(T)}{dT}. \quad (2)$$

### III. RESULTS AND DISCUSSION

We first searched for the equilibrium structures of three kinds of graphyne, which are indispensable to their phonon dispersion relations and thermal properties. Graphyne can be made by replacing all or some bonds in graphene by an AL ( $-\text{C}\equiv\text{C}-$ ). Among numerous different types of graphyne produced in this way, we only focused on three types of graphyne,  $\alpha$ ,  $\beta$ , and  $\gamma$ , which are highly symmetric in a hexagonal lattice relative to the other types. The  $\alpha$ -graphyne can be made by a complete substitution for graphitic bonds, while the  $\beta$ -graphyne and  $\gamma$ -graphyne can be formed by two-thirds and one-third substitutions, respectively. In these types of graphyne, there are at most three nonequivalent carbon-carbon bonds,  $d_1$ ,  $d_2$ , and  $d_t$ . Single-bond like  $d_1$  and  $d_2$  represent bonds from a  $sp^2$  atom to a neighboring  $sp$  and  $sp^2$  atom, respectively, while a triple-bond  $d_t$  describes a bond between two neighboring  $sp$  atoms forming an AL together with two  $d_1$  bonds.

For each graphyne, we completely scanned the whole energy surface while adjusting the bond length of three nonequivalent carbon-carbon bonds,  $d_1$ ,  $d_2$ , and  $d_t$  keeping its hexagonal symmetry. Note that there are no  $d_2$  bonds in  $\alpha$ -graphyne, and the lattice constant of each unit cell is uniquely determined for each set of given  $d_1$ ,  $d_2$ , and  $d_t$ . The equilibrium structures of three types of graphyne were determined at the minimum energy point in each energy surface, and shown in Fig. 1(a-c), where their hexagonal lattices were depicted by dashed parallelograms representing their unit cells. Two nonequivalent bonds in the  $\alpha$ -graphyne were calculated to be  $d_1 = 1.397$  Å and  $d_t = 1.230$  Å with lattice constant of  $a_{\text{eq}} = 6.969$  Å. For the  $\beta$ -graphyne ( $\gamma$ -graphyne), on the other hand, its calculated lattice constant and three nonequivalent bond lengths are  $a_{\text{eq}} = 9.480$  Å (6.890 Å),  $d_1 = 1.389$  Å (1.408 Å),  $d_2 = 1.458$  Å (1.426 Å), and  $d_t = 1.232$  Å (1.223 Å). Our determined structural parameters are in good agreement with other studies. [18, 21]

To compare the structural stability of three types of graphyne, we evaluated their cohesive energies with respect to that of graphene as a function of  $N_{sp}/N$ , where  $N_{sp}$  and  $N$  are the

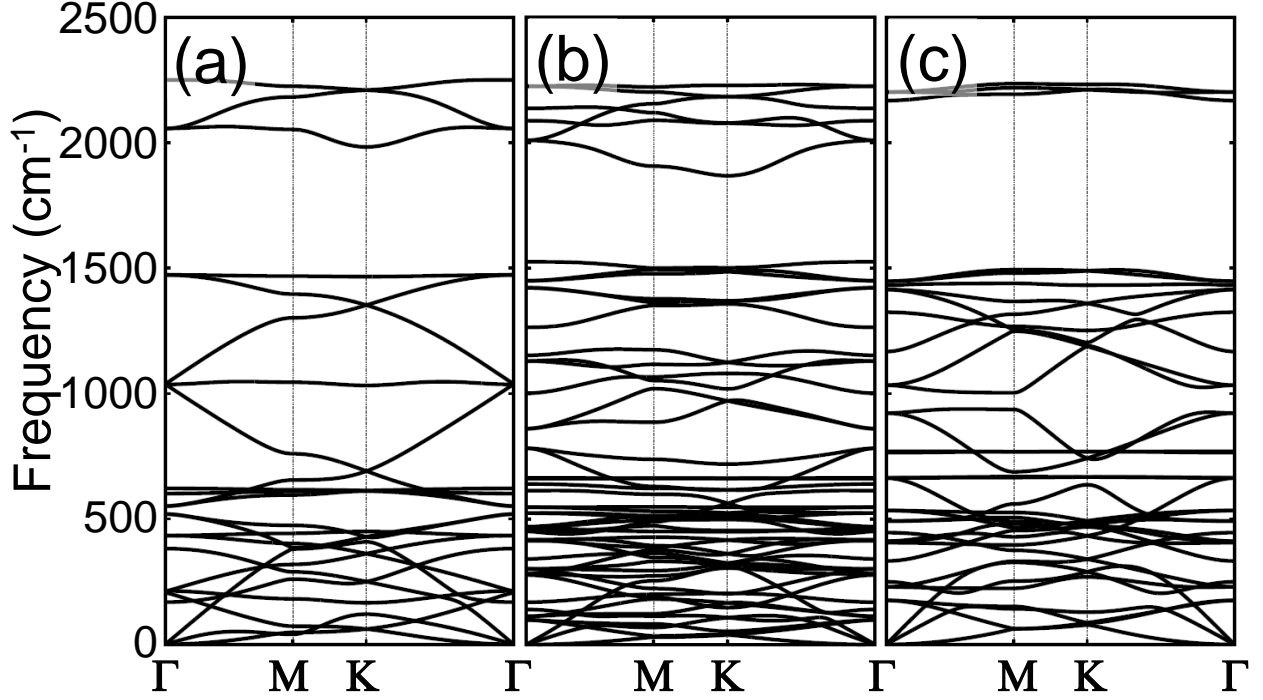


FIG. 2. The phonon dispersion relations of (a)  $\alpha$ -graphyne, (b)  $\beta$ -graphyne, and (c)  $\gamma$ -graphyne along the high symmetry lines in 2D hexagonal Brillouin zones.

number of  $sp$ -bonded or doubly-coordinated atoms, and  $N$  and the total number of atoms in the unit cell, respectively. As displayed in Fig. 1(d), these types of graphyne are only  $0.6\text{--}0.8\text{ eV/atom}$  less stable than graphene. This tendency agrees well with quantum Monte Carlo calculations [27–29]. Especially, the  $\gamma$ -graphyne and  $\beta$ -graphyne are even more stable than graphdiyne, which was already reported to be synthesized, [25, 26] expecting to be synthesized as well.

Using  $3 \times 3 \times 1$ -repeated supercells of the equilibrium structures, we calculated the phonon dispersion relations of all three types of graphyne as shown in Fig. 2, and identified all the phonon branches by analyzing their corresponding eigenvectors. We found in all cases that there are three acoustic phonon branches below  $\nu \approx 400\text{ cm}^{-1}$ , two in-plane modes with a linear dispersion and one quadratic out-of-plane mode near  $\Gamma$  point. We did not find any imaginary frequencies in all the types of graphyne indicating their structural stability. Note that there were inconsistent results for  $\beta$ -graphyne in previous studies showing imaginary phonon frequencies [21] or phonon mode anomalies, [20] which were not observed in our calculation. We believe that such inconsistency was due to use of an incompletely relaxed

structure in a small supercell size. On the other hand, the calculated phonon dispersion relations of  $\alpha$ -graphyne and  $\gamma$ -graphyne are in good agreement with other studies. [20, 21]

Compared to graphene with its maximum frequency of  $\lesssim 1600 \text{ cm}^{-1}$ , [61] graphyne exhibits even higher phonon branches dispersed at  $\nu \gtrsim 2000 \text{ cm}^{-1}$ . These high frequency modes correspond mainly to the stretching vibration of the triple bonds  $d_t$  with larger force constants than single-bond-like  $d_1$  and  $d_2$ , which generate graphene-like phonon modes at  $\nu \lesssim 1500 \text{ cm}^{-1}$  below a large frequency gap of  $\Delta\nu \approx 500 \text{ cm}^{-1}$ , as displayed in Fig. 2. The existence of such a large frequency gap implies that the vibration of  $d_t$  bond stretching modes is strongly protected from being scattered by the graphene-like modes by the energy conservation law. [62] Another phonon gap of  $\Delta\nu \approx 32, 78, \text{ or } 67 \text{ cm}^{-1}$ , was also observed near  $\nu \approx 500, 750, \text{ or } 1000 \text{ cm}^{-1}$  for  $\alpha$ -,  $\beta$ -, or  $\gamma$ -graphyne, respectively. We found that the  $d_1$  and  $d_2$  stretching modes are dispersed above the gap, while all the bending modes including optical flexural modes are settled below. Note there is an exception in the  $\alpha$ -graphyne as displayed in Fig. 2(a) that there are two flat modes identified as optical flexural modes located at  $\nu \approx 602$  and  $622 \text{ cm}^{-1}$  above the gap. Therefore, in the  $\alpha$ -graphyne, these optical flexural phonons can be scattered by the stretching phonons, while in the other types of graphyne, they are located at similar frequencies, but below their frequency gap, as shown in Fig. 2(b) and (c), which protects them from being scattered by their corresponding  $d_1$  and  $d_2$  stretching modes.

To evaluate the Helmholtz free energy, we used Eq. (1) with the phonon dispersion relations  $\omega_{\mathbf{q},n}$  calculated at 12 different area points, based on QHA. For each type of graphyne, the calculated Helmholtz free energy was plotted as a function of temperature and area in a color-coded map as displayed in Fig. 3. Note that color-coded energy values clearly represent that the  $\gamma$ -graphyne is more stable than the other two types. The temperature dependence of the equilibrium area  $A(T)$  was obtained by minimizing the thermodynamic functions with respect to the area as denoted with the black solid line on each color-coded map in Fig. 3.

We explored the TE behaviors of three types of graphyne as well as graphene for comparison by evaluating the temperature dependence of change in each system's area with respect to the zero-temperature area,  $\Delta A/A_0 \equiv [A(T) - A_0]/A_0$ , and its area TEC  $\alpha_s(T)$  given by Eq. (2). It was found that similar to graphene, all three types of graphyne contract as temperature increases up to  $T \approx 1000 \text{ K}$ , as shown in Fig. 4(a). Such an area shrink



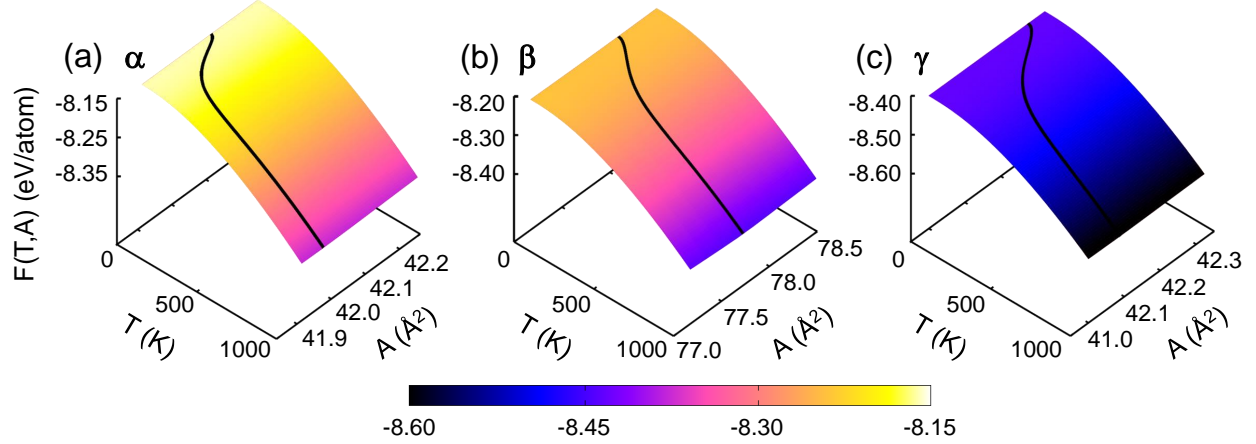


FIG. 3. (Color online) Color-coded maps of Helmholtz free energy of (a)  $\alpha$ -graphyne, (b)  $\beta$ -graphyne, and (c)  $\gamma$ -graphyne as a function of temperature and area calculated using Eq. 1. The black solid line on each plot indicates minimum value of free energy at each given temperature with respect to the area, and thus the equilibrium area for a given temperature. The color-coded free energy values are given in the color bar below.

observed in a 2D sheet was attributed to its flexural modes, which are mainly responsible for the ripple effect, [63] as in graphene, [30, 61] and in graphyne. [21, 30] We confirmed the contribution of flexural modes of graphyne to NTE by evaluating their corresponding mode Grüneisen parameters,  $\gamma_{\mathbf{q},n}$ , defined as

$$\gamma_{\mathbf{q},n} = -\frac{\partial \log \omega_{\mathbf{q},n}}{\partial \log V} = -\frac{V}{\omega_{\mathbf{q},n}} \frac{\partial \omega_{\mathbf{q},n}}{\partial V}, \quad (3)$$

to be negative.

Using Eq. (2), we also calculated the TECs of three types of graphyne as well as graphene. Compared to our calculated TEC values of graphene, which are in good agreement with previous studies, [30, 61] it was observed that graphyne exhibits significantly lower TEC values than graphene as shown in Fig. 4(b), which cannot be fully understood only by the flexural modes responsible for the ripple effect. To scrutinize such large differences, we thoroughly inspected the real-space vibrations of all the phonon modes by visualizing their corresponding eigenvectors together with mode Grüneisen parameters at different wave vectors  $\mathbf{q}$  and mode indices  $n$ , and found intriguing unexpected vibrational modes, which we classified as RUMs. [40] It has already been known that the RUMs and quasi RUMs (qRUMs) involving a little distortion of rigid polyhedra are major causes of NTE occurred in an oxide framework consisting of rigid polyhedra, such as  $\text{MO}_4$  and  $\text{MO}_6$ , where M and

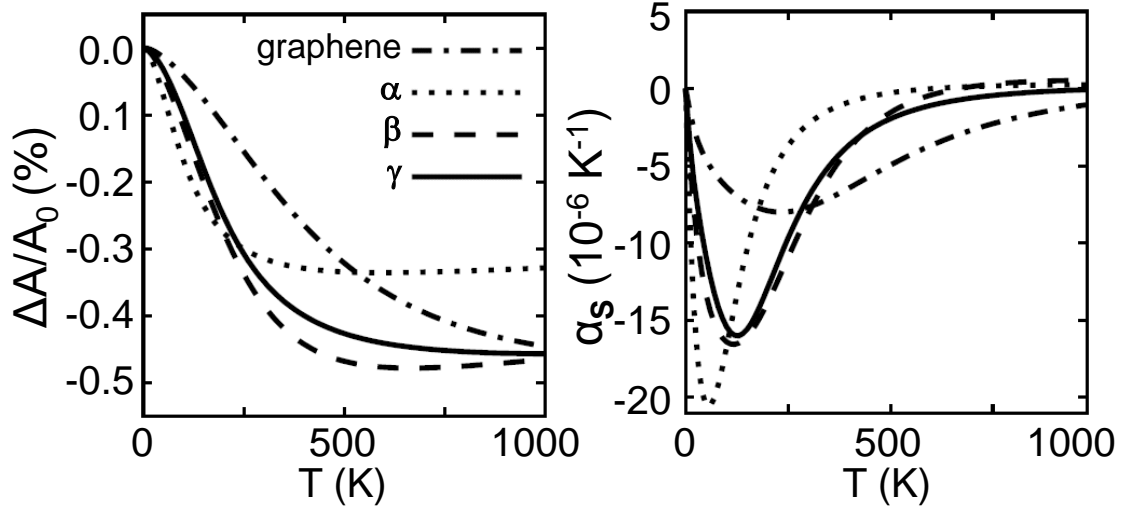


FIG. 4. (a) Temperature dependence of the ratio of area expansion to the reference area at  $T = 0$  K,  $\Delta A/A_0$  in the unit of percentage %, and (b) the corresponding area thermal expansion coefficient,  $\alpha_s(T)$ , defined by Eq. 2, in the unit of  $10^{-6} \text{ K}^{-1}$ , of  $\alpha$ -graphyne (dotted line),  $\beta$ -graphyne (dashed line), and  $\gamma$ -graphyne (solid line) as well as of graphene (dash-dotted line) for comparison.

O are a metal cation and oxygen, [64, 65] although it was reported that there is no simple correlation between NTE and RUMs. [66]

Fig. 5(a–c) shows real-space visualization of typical RUMs (in the right) observed at  $\nu \approx 382$ , 277, and  $249 \text{ cm}^{-1}$  in  $\alpha$ -,  $\beta$ -, and  $\gamma$ -graphyne, respectively, in tandem with their corresponding equilibrium configurations (in the left). The corresponding rigid units are denoted respectively by gray polygons of a triangle, a rectangle, and a hexagon, each of which encloses the  $sp^2$  carbon atoms connected with  $d_1$  and  $d_2$  bonds. During the libration mode of the rigid unit in each graphyne, every AL becomes bended and thus the  $d_t$  bonds are lengthened as shown in Fig. 5(a–c). We found that such lengthened bonds can be compensated by filling an empty space or reducing the area size. To clarify the correlation between these RUMs and NTE in the graphyne systems and to analyze the size reduction quantitatively, we calculated the relative energy of each type of graphyne as a function of the area change  $\Delta A/A_0$  with respect to the zero-temperature area  $A_0$ , and the rotation angle  $\varphi$  of each rigid unit. Fig. 5(d–f) displays the color-coded energy map, in which the area reduction was estimated by searching for the minimum values of the relative energy  $\Delta E$  for a given  $\varphi$ , as depicted with cyan-colored line with dots. Since the maximum rotation

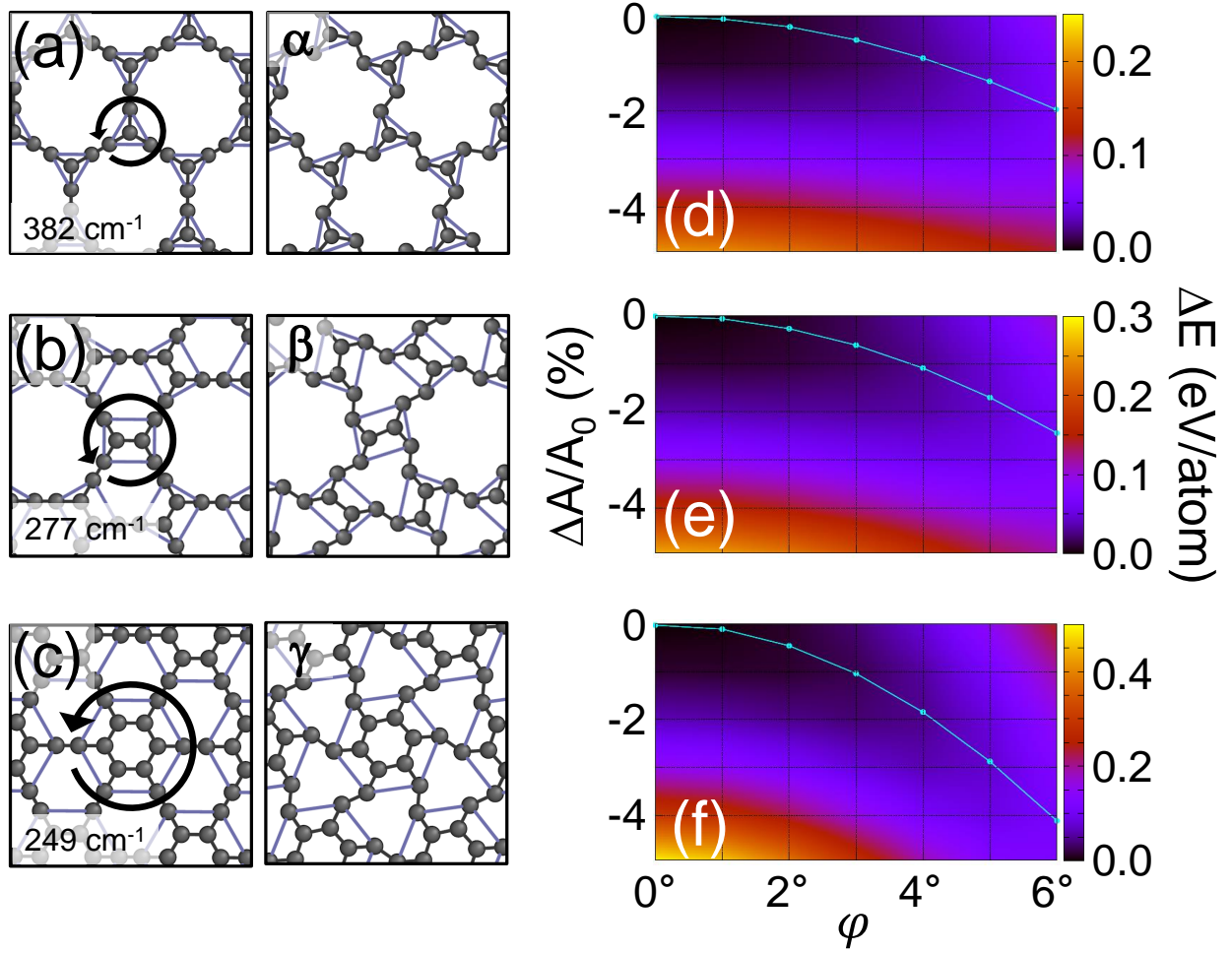


FIG. 5. Real-space visualization of typical rigid unit modes observed in (a)  $\alpha$ -graphyne (b)  $\beta$ -graphyne, and (c)  $\gamma$ -graphyne respectively with  $\nu \approx 382, 277$  and  $249 \text{ cm}^{-1}$ . Each local rigid unit is represented by gray polygon (triangle, square, or hexagon in (a), (b), or (c), respectively) surrounding  $sp^2$  carbon atoms with  $d_1$  and  $d_2$  bonds. Each equilibrium structure is depicted in the left box, while the right box shows a snapshot of rigid units rotated counterclockwise corresponding to the selected RUM. Relative energy map color-coded as a function of  $\Delta A/A_0$  and rotation angle  $\varphi$  of each rigid unit calculated for (d)  $\alpha$ -graphyne, (e)  $\beta$ -graphyne, and (f)  $\gamma$ -graphyne. Cyan-colored solid line with dots indicates the area contraction determined by the minimum energy for given  $\varphi$ . Energy values are given in terms of the equilibrium energy of each graphyne.

angle may increase with temperature, RUMs as well as the ripple effects may contribute to the area reduction. The mode Grüneisen parameters corresponding the RUMs was also calculated to be negative as similarly in the flexural modes contributing to the ripple effects.

#### IV. CONCLUSIONS

We presented the phonon dispersion relations and the thermal expansion behaviors of  $\alpha$ -,  $\beta$ - and  $\gamma$ -graphyne using the density functional theory. Our calculated phonon dispersion relations showed that there were no imaginary frequencies implying their structural stability. Their high-frequency modes at  $\nu \approx 2000 \text{ cm}^{-1}$  correspond to the stretching modes of the triple bonds  $d_t$ , which are protected by the large frequency gap from being scattered by graphene-like modes of  $d_1$  and  $d_2$  bonds. Similarly, the stretching modes of  $d_1$  and  $d_2$  bonds can also be protected from being scattered by their bending modes, since the latter modes are separately located below another frequency gap, with an exception in  $\alpha$ -graphyne. Our quasi harmonic approximation calculations revealed that all types of graphyne exhibit negative thermal expansion as in other 2D materials, but they have much larger values in negative thermal expansion coefficients than graphene. This significant discrepancy was resolved by identifying the rigid unit modes, which were firstly observed in 2D carbon graphitic structures. We found that not only the ripple effect originating from the flexural modes, but also the rigid unit modes are strongly responsible for the negative thermal expansion in graphyne.

#### ACKNOWLEDGMENTS

We thank Mr. Hyeonsu Lee for fruitful discussion. We acknowledge financial support from the Korean government through National Research Foundation (NRF-2015R1A2A2A01006204). Some portion of our computational work was done using the resources of the KISTI Super-computing Center (KSC-2014-C2-028 and KSC-2014-G2-001).

---

[1] H. W. Kroto, J. R. Heath, S. C. O'Brien, R. F. Curl, and R. E. Smalley, *Nature* **318**, 162 (1985).

- [2] S. Iijima, *Nature* **354**, 56 (1991).
- [3] K. S. Novoselov, A. K. Geim, S. V. Morozov, D. Jiang, Y. Zhang, S. V. Dubonos, I. V. Grigorieva, and A. A. Firsov, *Science* **306**, 666 (2004).
- [4] Y. Zhang, Y.-W. Tan, H. L. Stormer, and P. Kim, *Nature* **438**, 201 (2005).
- [5] K. S. Novoselov, A. K. Geim, S. V. Morozov, D. Jiang, M. I. Katsnelson, I. V. Grigorieva, S. V. Dubonos, and A. A. Firsov, *Nature* **438**, 197 (2005).
- [6] A. H. Castro Neto, N. M. R. Peres, K. S. Novoselov, A. K. Geim, and F. Guinea, *Rev. Mod. Phys.* **81**, 109 (2009).
- [7] H. Şahin and S. Ciraci, *Phys. Rev. B* **84**, 035452 (2011).
- [8] S. Kim, J. Ihm, H. Choi, and Y.-W. Son, *Phys. Rev. Lett.* **100**, 176802 (2008).
- [9] Y.-W. Son, M. L. Cohen, and S. G. Louie, *Phys. Rev. Lett.* **97**, 216803 (2006).
- [10] S. Y. Zhou, G.-H. Gweon, A. V. Fedorov, P. N. First, W. A. de Heer, D.-H. Lee, F. Guinea, A. H. Castro Neto, and A. Lanzara, *Nat. Mater.* **6**, 770 (2007).
- [11] Y.-K. Kwon, *J. Korean Phys. Soc.* **57**, 778 (2010).
- [12] J. Haskins, A. Kınacı, C. Sevik, H. Sevincli, G. Cuniberti, and T. Cagn, *ACS Nano* **5**, 3779 (2011).
- [13] A. Hirsch, *Nat. Mater.* **9**, 868 (2010).
- [14] R. H. Baughman, *J. Chem. Phys.* **87**, 6687 (1987).
- [15] J. Kang, J. Li, F. Wu, S.-S. Li, and J.-B. Xia, *J. Phys. Chem. C* **115**, 20466 (2011).
- [16] J. Zhou, K. Lv, Q. Wang, X. S. Chen, Q. Sun, and P. Jena, *J. Chem. Phys.* **134**, 174701 (2011).
- [17] D. Malko, C. Neiss, F. Viñes, and A. Görling, *Phys. Rev. Lett.* **108**, 086804 (2012).
- [18] B. G. Kim and H. J. Choi, *Phys. Rev. B* **86**, 115435 (2012).
- [19] Z. Liu, G. Yu, H. Yao, L. Liu, L. Jiang, and Y. Zheng, *New J. Phys.* **14**, 113007 (2012).
- [20] V. N. Popov and P. Lambin, *Phys. Rev. B* **88**, 075427 (2013).
- [21] N. K. Perkgöz and C. Sevik, *Nanotechnology* **25**, 185701 (2014).
- [22] E. L. Spitler, C. A. J. Li, and M. M. Haley, *Chem. Rev.* **106**, 5344 (2006).
- [23] M. M. Haley, *Pure Appl. Chem.* **80**, 519 (2008).
- [24] T. Takeda, A. G. Fix, and M. M. Haley, *Org. Lett.* **12**, 3824 (2010).
- [25] G. Li, Y. Li, H. Liu, Y. Guo, Y. Li, and D. Zhu, *Chem. Commun. (Camb)*. **46**, 3256 (2010).
- [26] X. Qian, Z. Ning, Y. Li, H. Liu, C. Ouyang, Q. Chen, and Y. Li, *Dalton Trans.* **41**, 730 (2012).

- [27] A. L. Ivanovskii, Prog. Solid State Chem. **41**, 1 (2013).
- [28] W.-J. Yin, Y.-E. Xie, L.-M. Liu, R.-Z. Wang, X.-L. Wei, L. Lau, J.-X. Zhong, and Y.-P. Chen, J. Mater. Chem. A **1**, 5341 (2013).
- [29] H. Shin, S. Kang, J. Koo, H. Lee, J. Kim, and Y. Kwon, J. Chem. Phys. **140**, 114702 (2014).
- [30] T. Shao, B. Wen, R. Melnik, S. Yao, Y. Kawazoe, and Y. Tian, J. Chem. Phys. **137**, 194901 (2012).
- [31] J. B. Nelson and D. P. Riley, Proc. Phys. Soc. **57**, 477 (1945).
- [32] Y.-K. Kwon, S. Berber, and D. Tománek, Phys. Rev. Lett. **92**, 015901 (2004).
- [33] Y.-K. Kwon, S. Berber, and D. Tománek, Phys. Rev. Lett. **94**, 209702 (2005).
- [34] C. Martinek and F. A. Hummel, J. Am. Ceram. Soc. **51**, 227 (1968).
- [35] Y. Long, N. Hayashi, T. Saito, M. Azuma, S. Muranaka, and Y. Shimakawa, Nature **458**, 60 (2009).
- [36] Y. Long and Y. Shimakawa, New J. Phys. **12**, 063029 (2010).
- [37] M. Azuma, W.-t. Chen, H. Seki, M. Czapski, S. Olga, K. Oka, M. Mizumaki, T. Watanuki, N. Ishimatsu, N. Kawamura, et al., Nat. Commun. **2**, 347 (2011).
- [38] T. Moriya and K. Usami, Solid State Commun. **88**, 911 (1993).
- [39] K. Sumiyama, M. Shiga, M. Morioka, and Y. Nakamura, J. Phys. F Met. Phys. **9**, 1665 (1979).
- [40] K. D. Hammonds, M. T. Dove, A. P. Giddy, V. Heine, and B. Winkler, Am. Mineral. **81**, 1057 (1996).
- [41] M. Tucker, A. Goodwin, M. Dove, D. Keen, S. Wells, and J. Evans, Phys. Rev. Lett. **95**, 255501 (2005).
- [42] J. Arvanitidis, K. Papagelis, S. Margadonna, K. Prassides, and A. N. Fitch, Nature **425**, 599 (2003).
- [43] C. E. Guillaume, CR Acad. Sci **125**, 18 (1897).
- [44] L. M. Sullivan and C. M. Lukehart, Chem. Mater. **17**, 2136 (2005).
- [45] C. Verdon, Scr. Mater. **36**, 1075 (1997).
- [46] H. Holzer and D. C. Dunand, J. Mater. Res. **14**, 780 (2011).
- [47] Z. W. Xue, L. D. Wang, Z. Liu, and W. D. Fei, Scr. Mater. **62**, 867 (2010).
- [48] M. Ishii, H. Shimojima, H. Takagi, K. Takenaka, and M. Watanabe, *Metal/ceramic composite material and process for production thereof* (2008).
- [49] A. L. Goodwin and C. J. Kepert, Phys. Rev. B **71**, 140301 (2005).

- [50] W. Kohn and L. J. Sham, Phys. Rev **385** (1965).
- [51] G. Kresse and J. Furthmüller, Phys. Rev. B. Condens. Matter **54**, 11169 (1996).
- [52] G. Kresse and J. Hafner, Phys. Rev. B **47** (1993).
- [53] P. E. Blöchl, Phys. Rev. B **50**, 17953 (1994).
- [54] G. Kresse and D. Joubert, Phys. Rev. B **59**, 11 (1999).
- [55] J. P. Perdew, K. Burke, and M. Ernzerhof, Phys. Rev. Lett. **77**, 3865 (1996).
- [56] K. Parlinski, Z. Li, and Y. Kawazoe, Phys. Rev. Lett. **78**, 4063 (1997).
- [57] A. Togo, F. Oba, and I. Tanaka, Phys. Rev. B **78**, 134106 (2008).
- [58] P. Pavone, K. Karch, O. Schütt, and D. Strauch, Phys. Rev. B **48**, 3156 (1993).
- [59] A. Togo, L. Chaput, I. Tanaka, and G. Hug, Phys. Rev. B **81**, 174301 (2010).
- [60] P. Vinet and J. H. Rose, J. Phys. Condens. Matter **1**, 1941 (1989).
- [61] N. Mounet and N. Marzari, Phys. Rev. B **71**, 205214 (2005).
- [62] J.-W. Jiang, Nanoscale **6**, 8326 (2014).
- [63] I. M. Lifshitz, Zh. Eksp. Teor. Fiz **22**, 475 (1952).
- [64] A. K. A. Pryde, K. D. Hammonds, M. T. Dove, V. Heine, J. D. Gale, and M. C. Warren, J. Phys. Condens. Matter **8**, 10973 (1996).
- [65] W. Miller, C. W. Smith, D. S. Mackenzie, and K. E. Evans, J. Mater. Sci. **44**, 5441 (2009).
- [66] J. Z. Tao and A. W. Sleight, J. Solid State Chem. **173**, 442 (2003).